Introduction

An accurate velocity model is the fundamental prerequisite for a high quality migration image. Until recently, such models were estimated by either migration velocity analysis (MVA) (Symes and Kern, 1994; Sava and Vlad, 2008) or traveltime tomography (Langan et al., 1984; Ivansson, 1985; Nemeth et al., 1997). These methods, however, only estimate velocity models with intermediate resolution compared to our demand for the highest resolution possible, particularly in imaging below complex geological features such as salt. To reconstruct the higher wavenumbers full waveform inversion (FWI) (Tarantola, 1984; Mora, 1987; Bunks et al., 1995; Zhou et al., 1995; Pratt, 1999; Shin and Ha, 2008; Krebs et al., 2009) uses both the phase and amplitudes to invert for a highly accurate velocity model. Today, this technology has matured to the point of providing reliable velocity models to a depth of several kilometers in sediments with intermediate complexity. However, it is still a challenge to accurately and reliably invert for velocities beneath salt and complex targets below 5 km or so. Part of the problem is that complex salt bodies defocus the incident energy below the salt and so the signal-to-noise ratio of subsalt reflections is too low for reliable inversion. Therefore, it is important to discover a means to provide greater seismic illumination below the salt that can enhance the estimation of subsalt velocities.

We propose FWI of data created by extended, rather than localized, sources at the surface so that the subsalt illumination is greatly enhanced. This follows the work of Liu et al. (2011) who migrated surface-related multiples to increase the illumination below salt. The extended source for FWI is created by treating each hydrophone as a virtual point source on the free surface, where the source wavelets are the upgoing reflections recorded by the hydrophones. This natural source of extended energy is numerically propagated as the source field and zero-lag correlated with the backpropagated multiples (recorded at the same hydrophones) to give the misfit gradient (or migration image). The 1st-order and higher-order reflections are extracted from the data by a surface-related multiple elimination method and have the potential to provide much more natural energy below the salt than a localized point source. Hence, the resulting subsalt reflections should have a higher SNR and subsurface coverage than those created by a single point source, and so enhance the capability of subsalt FWI. An added advantage of this method is that, unlike conventional FWI, knowledge of the source wavelet is not required because the recorded data are used for the source wavelet of the downgoing field. Finally, the surface-related multiples travel twice or more the distance of primaries. This means higher frequencies are attenuated and the wavepaths are greatly widened to provide a much lower wavenumber estimate of the velocity model. This can possibly provide a replacement for lower frequency sources.

This paper is divided into four sections. The first one is the introduction, which is followed by the theory for inverting extended source data for the subsurface velocity distribution. The misfit function only consists of surface-related multiples, so the inversion of these data by FWI will be denoted as multiples waveform inversion (MWI). The third section presents test results on synthetic data computed from the Marmousi2 model. Finally, a summary of this research is presented.

Method

The MWI algorithm is similar to that of FWI. The misfit function is $\varepsilon = \frac{1}{2}\sum_{\omega}\sum_{g}\sum_{s}|\Delta M(\omega,\mathbf{x}_g,\mathbf{x}_s)|^2$, where the data residual $\Delta M(\omega,\mathbf{x}_g,\mathbf{x}_s)$ is defined as $\Delta M(\omega,\mathbf{x}_g,\mathbf{x}_s) = M(\omega,\mathbf{x}_g,\mathbf{x}_s)_{cal} - M(\omega,\mathbf{x}_g,\mathbf{x}_s)_{obs}$, $M(\omega,\mathbf{x}_g,\mathbf{x}_s)_{cal}$ represents the predicted multiples related to the free surface, $M(\omega,\mathbf{x}_g,\mathbf{x}_s)_{obs}$ is the observed data. The misfit gradient $\gamma(\mathbf{x})$ is defined as:

$$\gamma(\mathbf{x}) = \frac{\delta\varepsilon}{\delta s(\mathbf{x})} = \sum_{\omega}\sum_{g}\sum_{s} Real[2\omega^2 s(\mathbf{x})G(\mathbf{x}|\mathbf{x}_g)\Delta M(\omega,\mathbf{x}_g,\mathbf{x}_s)^* \int G(\mathbf{x}|\mathbf{x}'_g)d(\omega,\mathbf{x}'_g,\mathbf{x}_s)d\mathbf{x}'_g], \qquad (1)$$

where, $\delta\varepsilon$ is the misfit perturbation, $\delta s(\mathbf{x})$ is the slowness perturbation, $G(\mathbf{x}'|\mathbf{x}'_g)$ is the Green's function for a source at $\mathbf{x}'_g$ and an observer at $\mathbf{x}'$ in the background velocity model, and $d(\omega,\mathbf{x}'_g,\mathbf{x}_s)$ is the recorded trace that serves as the time history of the virtual source at $\mathbf{x}'_g$ that includes primary and multiples. The

slowness can be iteratively updated by the steepest descent method, until the data residual falls below a specified limit.

Generation of predicted multiples

The predicted MWI data are the surface-related multiples, so their accurate calculation is crucial for the success of this method. Therefore, the first step is to forward model an extended line of virtual point sources at $\mathbf{x}_g$, each having the recorded data $d(\omega,\mathbf{x}_g,\mathbf{x}_s)$ as the time history for the same shot at $\mathbf{x}_s$. In this case, the extended virtual sources yield the wavefield $P(\omega,\mathbf{x}_g,\mathbf{x}_s)$ in the frequency domain as:

$$P(\omega,\mathbf{x}_g,\mathbf{x}_s) = \int G(\mathbf{x}_g|\mathbf{x}'_g)d(\omega,\mathbf{x}'_g,\mathbf{x}_s)d\mathbf{x}'_g. \tag{2}$$

Here, $G(\mathbf{x}_g|\mathbf{x}'_g)$ is the harmonic Green's function for a source at $\mathbf{x}'_g$ and an observer at $\mathbf{x}_g$, and $d(\omega,\mathbf{x}_g,\mathbf{x}_s)$ is the input trace that acts as the time history of the virtual point source. We decompose the Green's function into a sum of two terms:

$$G(\mathbf{x}_g|\mathbf{x}'_g) = G_0(\mathbf{x}_g|\mathbf{x}'_g) + G_1(\mathbf{x}_g|\mathbf{x}'_g), \tag{3}$$

where, $G_0(\mathbf{x}_g|\mathbf{x}'_g)$ represents the Green's function of the direct wave in a homogeneous medium filled with water, and $G_1(\mathbf{x}_g|\mathbf{x}'_g)$ represents the Green's function associated with the reflections wavefield in a half-space of water underlain by sediments. We will assume that $d(\omega,\mathbf{x}_g,\mathbf{x}_s)$ only contains the downgoing reflections from the free surface. Substituting equation 3 into equation 2 yields the new expression:

$$P(\omega,\mathbf{x}_g,\mathbf{x}_s) = \overbrace{\int G_0(\mathbf{x}_g|\mathbf{x}'_g)d(\omega,\mathbf{x}'_g,\mathbf{x}_s)d\mathbf{x}'_g}^{\textit{downgoing primary and multiples in water layer}} + \overbrace{\int G_1(\mathbf{x}_g|\mathbf{x}'_g)d(\omega,\mathbf{x}'_g,\mathbf{x}_s)d\mathbf{x}'_g}^{\textit{upcoming multiples in heterogeneous model}}. \tag{4}$$

Because the extended virtual sources have time histories corresponding to the upgoing primary and multiple reflections recorded at the surface, the first term in equation 4 generates downgoing primary and multiple reflections in a homogeneous water layer, and the second term only contains the upgoing multiple reflections from the heterogeneous background model. In order to compute the downgoing primary and multiples in the 1st term of equation 4, we solve the acoustic wave equation for a homogeneous model with water velocity v_0 to get the pressure field $P_0(\omega,\mathbf{x}_g,\mathbf{x}_s)$, which is the firt part in equation 4. Subtracting $P_0(\omega,\mathbf{x}_g,\mathbf{x}_s)$ from equation 4, the predicted $M(\omega,\mathbf{x}_g,\mathbf{x}_s)$ can be obtained as:

$$M(\omega,\mathbf{x}_g,\mathbf{x}_s) = P(\omega,\mathbf{x}_g,\mathbf{x}_s) - P_0(\omega,\mathbf{x}_g,\mathbf{x}_s) = \int G_1(\mathbf{x}_g|\mathbf{x}'_g)d(\omega,\mathbf{x}'_g,\mathbf{x}_s)d\mathbf{x}'_g. \tag{5}$$

Numerical example

In this section, MWI will be tested on synthetic data calculated for the Marmousi2 model shown in Figure 1a. The model size is 200 $\times$ 400 gridpoints with a gridpoint separation of 10 m. There are 200 shots and the streamer is 2 km long with a 10 m hydrophone spacing and a 20 m shot interval. Here, the predicted data for standard FWI are generated with free-surface boundary conditions and the predicted data for MWI is generated with absorbing boundary conditions that replace the free surface boundary condition. Figure 1b shows the initial velocity model after smoothing the true velocity model. Application of FWI and MWI to these synthetic data results in the FWI and MWI tomograms in Figures 1c and 1d, respectively. The circled areas show that the MWI tomogram is more accurate than the FWI tomogram. Figures 2a and 2b show the data and model residuals for both the MWI and FWI methods and suggest that MWI enjoys a faster reduction in the residual than FWI, and also provides a more accurate velocity model for the same number of iterations. For MWI, the reconstructed earth model must explain a more complex wavefield from an extended source compared to that from a localized point source. This means that there are a fewer number of models that are consistent with the complex data compared to

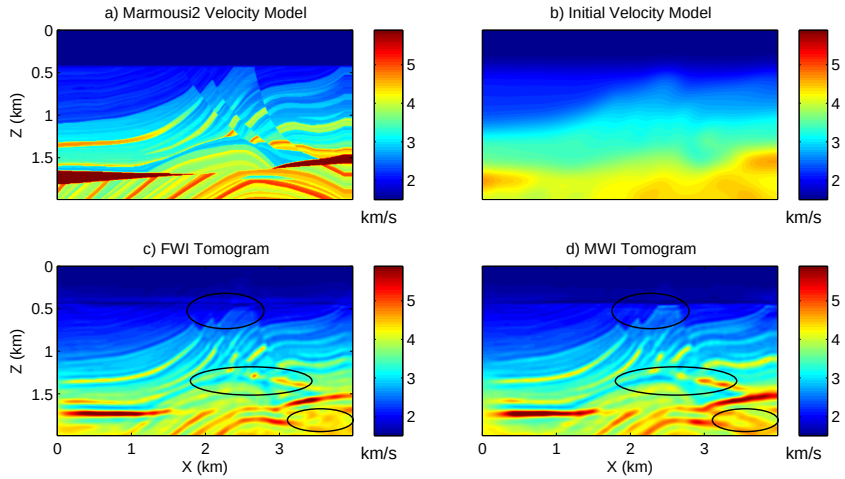

Figure 1 *a) Marmousi2 velocity model. b) Initial velocity model. c) FWI and d) MWI tomograms after 100 iterations.*

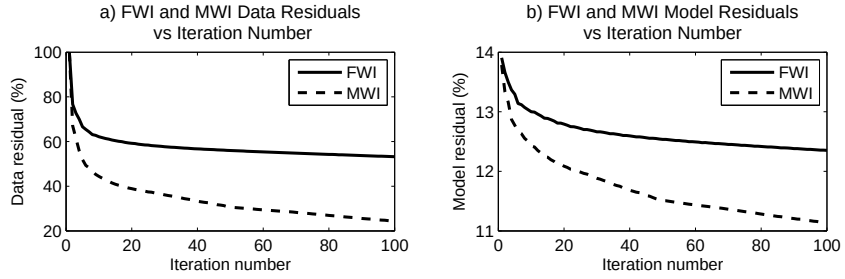

Figure 2 *a) Data and b) model residuals for FWI and MWI.*

the simpler point source data. This is similar to traveltime tomography where the data consist of simple traveltime picks at each trace, so many smooth models can easily explain the same simple data.

An advantage of MWI compared to FWI is that multiples from an extended source illuminate a much greater region in the subsurface compared to primaries associated with a localized source. This is illustrated in Figure 3ab where the misfit gradient from a CSG is compared to that from an extended source on the surface. It is obvious that the MWI gradient covers a much wider area in the subsurface than the FWI gradient. This suggests that after stacking, the subsurface MWI illumination will be wider and the SNR of the MWI image will be enhanced compared to that of the FWI image. If the streamer length increases, the extent of the MWI illumination zone will be even wider compared to the FWI zone, as illustrated in Figure 3cd.

Conclusions

We propose multiples waveform inversion to invert the surface-related multiples for the subsurface velocity distribution. In this method, recorded traces are used as the time histories of the virtual sources at the hydrophones and surface-related multiples are the observed data. For the field data, the recorded multiples can be obtained by a multiple filtering procedure such as the SRME method. In this paper, the observed multiples are calculated in the same way as the predicted multiples.

Numerical tests on the Marmousi2 model verify that MWI is a promising new method for velocity inversion. Compared to standard FWI, the advantages of MWI are that it uses the recorded trace as a source wavelet so no knowledge of the actual source wavelet is needed, and it enjoys faster convergence and higher resolution compared to FWI with the Marmousi2 data. A major benefit is that the extended

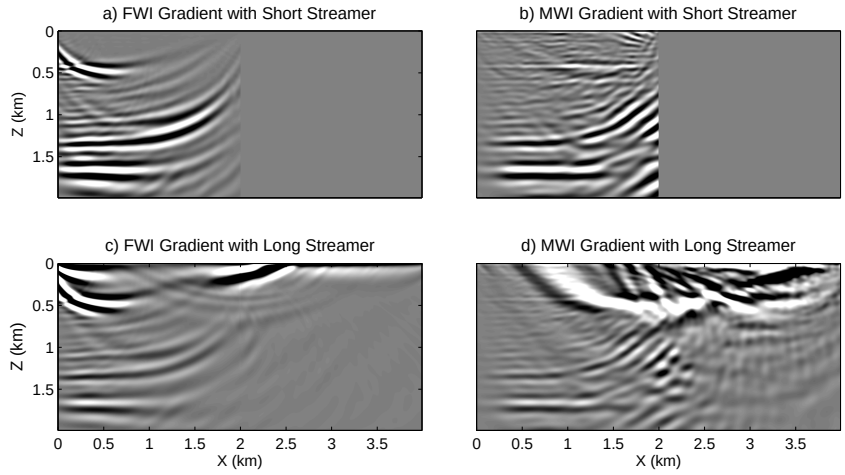

Figure 3 *a) FWI and b) MWI misfit gradients for synthetic data computed for a streamer with a length of 2 km. c) FWI and d) MWI misfit gradients for synthetic data computed for a streamer with a length of 4 km.*

source should provide much greater illumination of the subsurface compared to primary reflections, and an attendant improvement in imaging below salt.

Acknowledgements

We thank the KAUST Supercomputing Lab for the computer cycles they donated to this project. We are especially grateful for the use of the SHAHEEN supercomputer. We also acknowledge the support of the CSIM sponsors (http://csim.kaust.edu.sa).

References

Bunks, C., Saleck, F.M., Zaleski, S. and Chavent, G. [1995] Multiscale seismic waveform inversion. *Geophysics*, **60**(5), 1457–1473, doi:10.1190/1.1443880.

Ivansson, S. [1985] A study of methods for tomographic velocity estimation in the presence of low-velocity zones. *Geophysics*, **50**(6), 969–988, doi:10.1190/1.1441975.

Krebs, J.R. et al. [2009] Fast full-wavefield seismic inversion using encoded sources. *Geophysics*, **74**(6), WCC177–WCC188, doi:10.1190/1.3230502.

Langan, R.T., Lerche, I., Cutler, R.T., Bishop, T.N. and Spera, N.J. [1984] Seismic tomography: The accurate and efficient tracing of rays through heterogeneous media. *SEG Technical Program Expanded Abstracts*, **314**, 713–715, doi:10.1190/1.1894309.

Liu, Y., Chang, X., Jin, D., He, R., Sun, H. and Zheng, Y. [2011] Reverse time migration of multiples for subsalt imaging. *Geophysics*, **76**(5), WB209–WB216, doi:10.1190/geo2010-0312.1.

Mora, P. [1987] Nonlinear two-dimensional elastic inversion of multioffset seismic data. *Geophysics*, **52**(9), 1211–1228, doi:10.1190/1.1442384.

Nemeth, T., Normark, E. and Qin, F. [1997] Dynamic smoothing in crosswell traveltime tomography. *Geophysics*, **62**(1), 168–176, doi:10.1190/1.1444115.

Pratt, R.G. [1999] Seismic waveform inversion in the frequency domain, part 1: Theory and verification in a physical scale model. *Geophysics*, **64**(3), 888–901, doi:10.1190/1.1444597.

Sava, P. and Vlad, I. [2008] Numerical implementation of wave-equation migration velocity analysis operators. *Geophysics*, **73**(5), VE145–VE159, doi:10.1190/1.2953337.

Shin, C. and Ha, W. [2008] A comparison between the behavior of objective functions for waveform inversion in the frequency and laplace domains. *Geophysics*, **73**(5), VE119–VE133, doi:10.1190/1.2953978.

Symes, W.W. and Kern, M. [1994] Seismic migration : theory and practice. *Geophysical Prospecting*, **42**(6), 565–614, ISSN 1365-2478, doi:10.1111/j.1365-2478.1994.tb00231.x.

Tarantola, A. [1984] Inversion of seismic reflection data in the acoustic approximation. *Geophysics*, **49**(8), 1259–1266, doi:10.1190/1.1441754.

Zhou, C., Cai, W., Luo, Y., Schuster, G. and Hassanzadeh, S. [1995] Acoustic wave-equation traveltime and waveform inversion of crosshole seismic data. *Geophysics*, **60**(3), 765–773, doi:10.1190/1.1443815.